International Journal of Non-Linear Mechanics 46 (2011) 637–647

Contents lists available at ScienceDirect

International Journal of Non-Linear Mechanics

journal homepage: www.elsevier.com/locate/nlm

The growth of giant pumpkins: How extreme weight influences shape

David L. Hu [a,b,*], Paul Richards [a], Alexander Alexeev [a]

[a] School of Mechanical Engineering, Georgia Institute of Technology, 801 Ferst Drive, Atlanta, GA 30332-0230, USA
[b] School of Biology, Georgia Institute of Technology, 310 Ferst Drive, Atlanta, GA 30332-0230, USA

ARTICLE INFO

Available online 6 January 2011

Keywords:
Fruit
Growth
Deformation
Plasticity
Giant

ABSTRACT

Great morphological differences exist among fruits and vegetables. In this combined experimental and theoretical study, we predict pumpkin shape evolution and maximum size based on their material properties. Using time-lapse photography and measurements collected by volunteer farmers, we show that as pumpkins grow, they morph from spherical to pancake shapes, flattening up to 50% in height-to-width aspect ratio. By compressing whole pumpkins in material-testing machines, we find that the elastic response of the pumpkin is insufficient to account for the large deformations characteristic of large pumpkins. We hypothesize that pumpkin flattening is caused by the weight of the pumpkin retarding its normal growth processes. We test this hypothesis using a mathematical model that assumes plant growth is stimulated in response to a tensile yield stress. We are able to predict pumpkin shapes consistent with those observed. The observed growth plasticity allows the fruit to redistribute internal stresses, thereby growing to extreme sizes without breaking.

1. Introduction

The development of shape in plants is a century-old problem [1] that has made recent advances due to the combined interdisciplinary efforts of plant, molecular and mathematical biology. A challenge inherent to this problem is the multiple length scales involved, particularly in embryogenesis or fruit growth, where an ovary of characteristic size 100 μm−10 mm will reproduce over time to become a 10-cm fruit, or in the case of this investigation, a one-meter fruit. During this vast change in size, the plant genome regulates growth through feedback with the multi-parameter chemical and physical state of the fruit [2]. The chemical and biological changes in cells during growth [3,4] are beyond the scope of this study. Instead, we focus on the use of a simple computational model, which approximates elasto-plastic plant material, to investigate the mechanics of extreme growth.

Given the computational nature of our study, it is worthwhile to briefly review previous mathematical approaches here. Goriely et al. [5] and Taber [6] provide comprehensive reviews of continuum models used to model the growth of plant and animal tissues. A common theme among these models is the decomposition of strain into components due to elasticity and growth. In another study, Vandiver and Goriely [7] explain how differential growth in the plant can generates residual stresses, such as tension, and consequently how these tensions can rigidify and strengthen the plant. Dumais et al. [8] has shown how the behavior of certain materials like rubber balloons can be used as models for root tip growth. Coen et al. [9] review how the growth of blossoms can be computationally modeled using formulations of elasticity and growth rules. While most previous models take one-dimensional or two-dimensional approaches to growth, we take advantage of computational methods that are particularly suited for examining three-dimensional changes.

We apply a lattice spring method (LSM) [10,11], a computational model, to estimate pumpkin deformation. Originally derived for performing atomistic simulations [12], this method can be applied for modeling elastic solids in the continuum mechanics approximation [10,11,13]. Our computational lattice model constitutes a means for examining the influence of the visco-plastic properties [10] on development of fruit shapes under different environmental conditions. Furthermore, by removing individual bonds, LSM allows modeling of crack formation and propagation thorough solid materials [14,15]. Such a scenario is often observed in giant vegetables where cracks may appear as a result of the extremely fast growth.

The study of large organisms can provide us insight into the growth and stress limits of tissues and can provide useful testing grounds for hypotheses about biomechanics. The largest organisms such as trees and dinosaurs, push the envelope of growth, metabolic and respiratory processes occurring in the whole organism and its constituent cells. For instance, the maximum height of redwood trees is 130 m, due to the inability of trees to syphon water at these height [16]. Water-walking insects have a maximum size of 30 cm because of surface tension effects [17]; the maximum size of prehistoric and extant dragonflies is 1 m and 20 cm, respectively, because of

* Corresponding author at: School of Mechanical Engineering, Georgia Institute of Technology, 801 Ferst Drive, Atlanta, GA 30332-0230, USA.
Tel.: +1 404 894 0573.
E-mail address: hu@me.gatech.edu (D.L. Hu).

0020-7462/$ - see front matter © 2010 Elsevier Ltd. All rights reserved.
doi:10.1016/j.ijnonlinmec.2010.12.013

changes in atmospheric gas composition [18,19]. By considering the growth of large fruits, as will be done in this study, one can amplify the effects of gravity on their development. For all these organisms, mechanical forces determine their maximum size and, to some extent, their behavior. Since the length and time scales of these organisms exceed those of typical sizes, studying large organisms is inherently difficult and information on them is sparse. To study giant plants we are forced to accept the uncontrolled conditions in which they are bred and grown because of the great personal care required by farmers to ensure growth at these sizes.

Annual agricultural competitions starting in the 1800's and the introduction of the Guinness book of World Records [20] in 1951 have driven amateur farmers to breed fruits and vegetables for size (Fig. 1). Over the years, the largest fruits and vegetables entered in these contests have grown to 3–100 times their normal weight, increasing yearly: recent records show that onions can exceed 10 lb and carrots over 50 lb (Fig. 1). Fig. 2a shows the growth rate of several record-breaking fruits and trees [21,22]. The leader among these giant fruits and vegetables are pumpkins which can grow to over 1000 lb within 4 months, increasing in weight by nearly 50 lb per day, a rate comparable to that of the largest trees (the black squares in Fig. 2a). The fruits borne by pumpkin plants are indeed giants in the sense that they are up to 100 times larger than average fruits produced by normal pumpkin plants, as shown in Fig. 2a. While neither the genetics nor growth conditions for these plants are tightly controlled, current records indicate that giant pumpkins may indeed be among the largest and fastest growing organisms in the world.

The motivation for this study is the following observation: fruits and vegetables at large sizes have drastically altered shapes. As shown in Fig. 1, ground fruits tend to be squashed, in accordance with the compressive forces generated by self-weight. This tendency is also shown in Fig. 2b which shows the aspect ratio of fruits as they increase in size. Note the largest fruits like pumpkins decrease in height-to-width ratio by 50% as they grow. We hypothesize that the effects of gravity play a critical role in the development of these abnormal shapes.

The growth of giant pumpkins is discussed in popular literature [23] and online pumpkin growing networks, which result from the collaborative effort of hundreds of growers. We summarize their relevant natural history here, although we caution the reader as some of this information is necessarily anecdotal. Giant pumpkins are all bred from a single variety called "Atlantic Giant pumpkins," patented by Howard Dill in 1979. Since then, no other pumpkin variety has become a world champion and most contenders are descendants from this seed. A major contributing factor to the size of giant pumpkins is their prolonged growth cycle. They are typically sown in early May and harvested in late September, a complete growth cycle of 140–160 days, in excess of the 90–120 day cycle of normal pumpkins.

The giant pumpkin growth cycle is composed of three phases. In the first 10 days of growth, known as the seedling stage, the planted pumpkin seeds begin to sprout leaves. In the subsequent 60–70 days, known as the plant growth stage, the plant grows sufficiently to develop male and female flowers. Once their flowers are mated, the fruiting stage begins. During these 70–80 days, the giant pumpkin grows at rates greatly exceeding that of normal pumpkins.

Fig. 1. Giant fruits and vegetables. Hanging fruits include (a) Apples, (b) Lemons, (c) Jackfruit, (d) Sea coconut; Ground-level fruits/vegetables include (e) Squashes, (f) Watermelons, (g) Cabbage; Underground vegetables include (h) Onions, (i) Carrots, (j) Rutabaga, (k) Sweet potatoes. Gravitational forces cause these fruits/vegetables to have odd shapes at large sizes. Fruits suspended from trees are subject to tension forces and tend to be elongate. Ground-supported bodies, subject to compression, such as the squash, melons and leafy vegetables tend to be flat. Underground vegetables, supporting the weight of the surrounding soil, tend to grow radially outward rather than straight down. Images (a,b,e) re-printed courtesy of Guinness world records [20]; (e) grown and photographed by Dutch Brad; (c) by Louis Brown for EzineMark.com; (k) by Brendan Borrell of Scientific American; (f) by Staurt Bauer and Julie Morrison of the Flint Journal; and (g,i) grown and photographed by John Evans and the World Carrot Museum, UK.

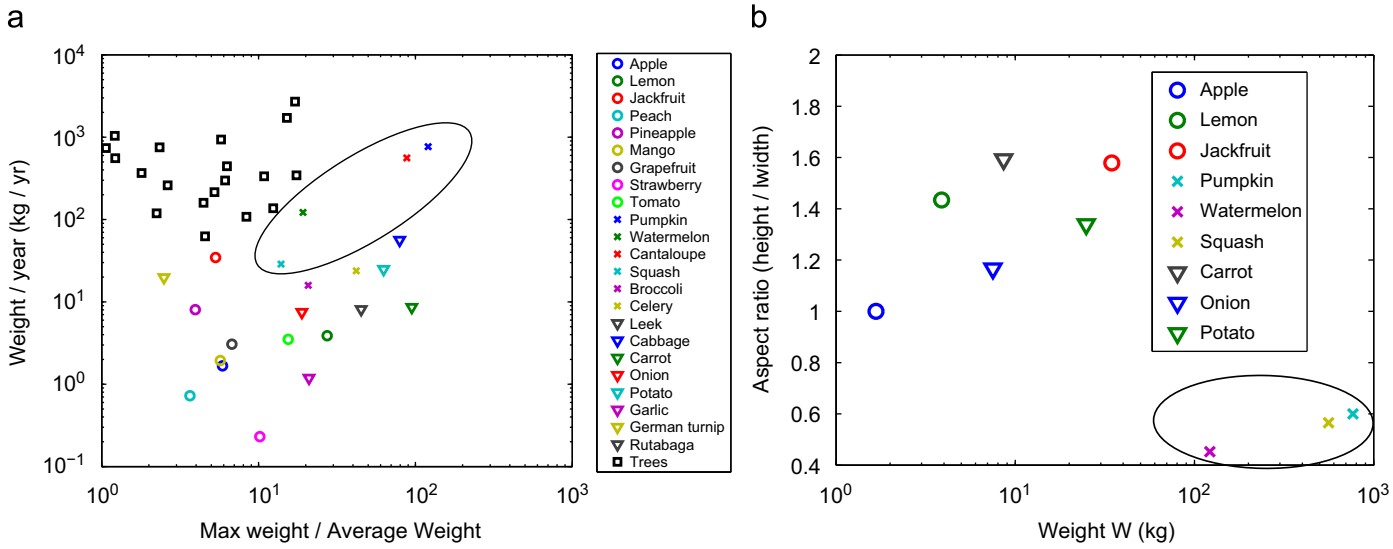

Fig. 2. (a) The relation between the growth rate (kg/year) and relative size of the largest plants in the world. Relative size is given in terms of the ratio between a plant's maximum and average weights. Note the pumpkins are in the upper right quadrant of the plot, indicating that they are among the largest and fastest growing plants. (b) The relation between aspect ratio (height/width) of a fruit to its maximum weight W (in kg). Pumpkins are in the lower right, indicating that they are the heaviest and flattest of the giant fruits. Average fruit weights and sizes were measured from a local supermarket, Guinness book of world records [20], and databases provided by nonprofit conservation organizations, such as The National Register of Big Trees (American Forests.org) [21], The Gymnosperm Database (Christopher J. Earle) [22], PLANTS database (USDA Natural Resources Conservation Services).

Pumpkins have attracted the interest of plant biologists and geneticists because of their great variety of shapes [24]. Taxonomically, pumpkins are a gourd-like squash of the genus *Cucurbita* and the family of gourds *Cucurbitaceae*. Edmund Sinnott wrote a number of classical papers (1936–1945) on the growth of *Cucurbita* that are worth reviewing here. In 1936, Sinnott [25] used breeding techniques to identify genes that explicitly govern pumpkin shape (width to height ratio). He considered two genetic lines of pumpkin, one shaped like a sphere and the other like a flying saucer, or "patty-pan." He found that the first generation (F1) was dominated by the spherical shape and the second generation (F2) was 3/4 disk and 1/4 sphere, as suggested by a single gene subject to Mendelian inheritance. In fact, Edmund states "the shape of the fruit is inherited independently of its size", where he defines a shape index as the ratio of length to width, the same index that we use in this investigation [26]. While Sinnott's observations is certainly true for low fruit-weights, we show in this study that fruits can become flattened as they increase in weight.

Pumpkins have a two-stage pattern of development that are common to other fleshy fruits [27,28]. In the first stage, the cells grow in number; in the second stage, they grow in size. Cell division rate is independent of cell size, despite that larger cells must gather more material before they can divide. Increase in cell size is interrupted at each division, in which each of the daughter cells assume half the volume of their parent cell. After the last cell division, increases in fruit size result exclusively from increases in cell size. The sizes of cells can vary, depending on their position within the fruit. For example, pumpkin cells decrease in size from the inside to the outside of the fruit (as in berry, cucumber and grape), whereas in apples, cells in the core are smallest. As the pumpkin diameter grows from 2 to 100 mm, cells on the endocarp (inside surface) of pumpkins can increase from 20 to 400 μm, whereas cells at the epidermis (outside surface) may either decrease or stay the same size.

Sinnott [27] studied the cells of both large-fruited (300 mm fruit diameter) and small-fruited pumpkins (100 mm diameter). Larger-fruit types have larger ovaries (22 mm) compared to smaller fruit-types (11 mm), while the ovarian cells in these types are approximately the same size ($\pm 5\%$). Larger fruits have a duration of cell division that is 5 times longer than that for small fruits, consequently leading to a greater number of cells produced. Moreover, larger fruits also have a greater degree of cell expansion than smaller fruits. For similar trends for other fruits, the reader is encouraged to consult the review by Coombe [28].

Cell shape is generally independent of fruit shape, with most cells being roughly spherical, be it in flat, spherical or bottle-shaped pumpkins. Histological studies [26] have shown that the change in shape is governed by differences in division rates along the axes of the fruit. For example, in flat pumpkins, cells tend to divide more frequently in the plane defining the widest region of the pumpkin. Sinnott [25] finds that the pumpkin grows in such a way that its length L and width W of the fruit are related by the power law $L \sim W^k$ where the allometric constant k differs between each line of pumpkin. Other geometric variables, such as the width of the upper lobe of bottle gourds, are also related to gourd length according to their own allometric constants. In our study, we will pay particular attention to characterizing gourd thickness (Fig. 3), a variable that is intimately linked to the strength of the fruit, but has otherwise received little attention by previous investigators.

Cellular growth is driven by turgor pressure inside the cell, which results from the cell varying its solute concentration and hydraulic conductance [8]. When turgor pressure is reduced to less than 30–50% of its normal value, cell expansion stops completely indicating that some threshold level of turgor pressure (yield stress) is necessary to drive wall extension [29]. This behavior is accounted for in the Bingham model [5] for viscoplastic growth,

$$\dot{\varepsilon} = \Phi(\sigma - \sigma_y), \quad \sigma \geq \sigma_y \tag{1}$$

where $\dot{\varepsilon}$ is the strain rate, Φ is the material extensibility (inverse viscosity), σ is the stress and σ_y is the yield stress. We assume that the pumpkin grows quasi-statically, so that we can neglect time-dependence. The constitutive relation for this plastic behavior is then

$$\sigma = \begin{cases} E\varepsilon & \text{if } \varepsilon < \varepsilon_y \\ E\varepsilon_y & \text{if } \varepsilon \geq \varepsilon_y \end{cases} \tag{2}$$

for axial loads. Physically, elastic deformation (of cell wall material) is associated with the reversible stretching (or uncoiling) of the

Fig. 3. Pumpkins ((a) whole and (b) in cross-section) increasing in diameter L from 6 to 140 cm. Scale bars, 10 cm. Note that the pumpkins begin growing spherically, but flatten as they reach maximum size.

(hemicellulose) bonds linking microfibrils [30]. Plastic deformation occurs when these bonds rupture and allows microfibrils to slide against each other. The result is permanent deformation when the material is unloaded [31]. This yield stress model is similar to the Lockhart equation of plant growth [32,33], in which a threshold turgor pressure is needed to generate yielding of the cell wall (a volumetric strain). The growth of pumpkins, as with other fruits, relies upon the dual processes of cellular expansion and cellular division. The former process is driven by turgor pressure. However, the latter process may be influenced by gravitational force. This force is larger in giant pumpkins, manifesting itself as abnormally large tensile and compressive stresses on the pumpkin bottom and top, respectively. As a result, normal cellular division processes may be interrupted or accelerated, resulting in anomalous shapes of the fruit.

2. Methods

2.1. Giant pumpkin measurements

We recruited 50 volunteer farmers (listed in the acknowledgements section) to share with us data on their giant pumpkins. Giant pumpkins of assorted strains were grown in the Northeastern United States in the months of July through October during the years 2002–2009. Pumpkins were positioned so that the stem-blossom axis was parallel to the ground. Methods on watering, fertilizing, shading and care for giant pumpkins are given in Langevin [23] and online. At the end of the growing season, giant pumpkins were weighed using balances provided at agricultural competitions.

The weight of five pumpkins was also monitored daily by a volunteer (Andy Wolf) during the growth season. Here, pumpkin weight is estimated according to so-called *giant pumpkin weight tables*, a standardized method of pumpkin weight-estimation accepted by the giant-pumpkin growing community. These tables list correlations between pumpkin weights and external measurements of their dimensions, first developed in 2001 by Len Stellpflug [23]. These tables were created using a polynomial regression to determine a best fit for 1194 sets of pumpkin dimensions and weights ranging between 0.2 and 408 kg. Details on the accuracy of this method were not available. However, we note that method has met the stringent needs of the competitive growing community for over a decade.

If the pumpkin were simply spherical, a single measure of the circumference would suffice to determine its weight, given the pumpkin's density. However, the pumpkins are often flattened at large sizes. Consequently, the pumpkin's weight is estimated using the average of three measures of the pumpkin's circumference (at mutually perpendicular directions, all with their origin in the center of the pumpkin). The first measurement is the *circumference*, measured in a horizontal plane parallel to the ground. The next two measurements are measured vertically by placing a tape measure across the pumpkin and the ends of the tape measure perpendicular to the ground. The first of these include the *over-the-top* measurement, in which the measurement is done along the stem-blossom axis. The second, the *side-to-side* measurement, is measured perpendicular to the stem-blossom axis, often along the pumpkin's widest girth. The change in these variables with respect to time will be shown in our results.

At the end of the growing season, pumpkins were bisected, through the plane formed by the direction of gravity and the stem-blossom axis. Cross-sections of the pumpkins were photographed and rulers and tape measures were used to measure the thicknesses, diameters and heights of the pumpkins. Data from volunteer farmers was combined with daily time-lapse videography of a single giant pumpkin filmed by a volunter, Ryan Foss [34]. The video is shown in the Supplementary Video section.

2.2. Instron experiments

Twenty-four pumpkins of diameter 6–30 cm were purchased from our local supermarket (in Atlanta). The pumpkins investigated in this study include the cultivars (cultivated plant varieties) of any one of the species *Cucurbita pepo, Cucurbita mixta, Cucurbita maxima,* and *Cucurbita moschata*. Ten pumpkins were cut into cross-section and their weight and dimensions measured using a laboratory scale and calipers. Using the remaining 14 pumpkins, we measured the stress and deformation response of pumpkins (of weights ranging from 2.7 and 8.6 kg) squeezed between two rigid plates in an Instron material-testing machine (inset of Fig. 8). The Instron was strain-controlled, applying sufficient force to increase in strain by 1% strain every minute. Tests were terminated once an audible cracking of the pumpkin occurred.

We note that the twenty-four pumpkins assayed using the Instron may be from different breeds. They thus may have values of elastic modulus, yield strain and fracture stress that are different from those of giant Atlantic pumpkin. Regretfully, measuring the material properties of actual giant pumpkins is quite difficult and

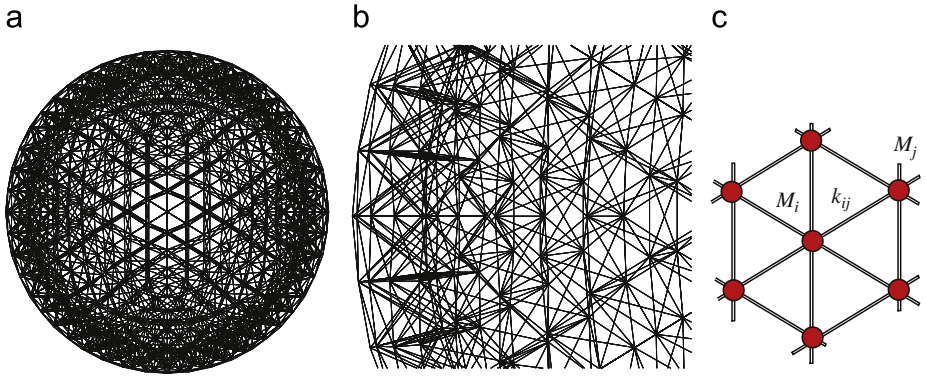

Fig. 4. The lattice spring network used to model the mechanics of the pumpkin shell. Masses M_i and M_j are connected by a spring with constant k_{ij}. A reduced number of nodes, with respect to the model, reported.

nearly impossible. There are very few samples available, which are spread out across the United States, making it difficult to collect rigorous data on different sizes. We hypothesize that our measurements for E and ε_y are correct within an order of magnitude. As is shown in our elastic deformation data (the red dashed lines) in Fig. 10, there is a common trend among the 24 pumpkins we studied. This indicates that the material properties among our sampled pumpkins are reasonably close in value.

2.3. Computational model

We model pumpkins as deformable spherical shells, whose geometry is characterized by a height H, diameter L and thickness of the shell t, as shown by the schematic in the inset of Fig. 7. Deformation of the pumpkin is caused by a gravitational force per unit volume ρg where $\rho \approx 1.0\,\mathrm{g/cm^3}$ is the density of the pumpkin [35] and $g \approx 9.8\,\mathrm{m/s^2}$ the gravitational acceleration. The pumpkin resists this gravitational force by elastic deformation of its material.

As external forces increase, plant cells continue to stretch until they exhibit a permanent tensile strain. In biology, the onset of plastic deformation is defined as when residual strain exceeds 0.01 (given for generic plant materials by [30,28]). We therefore estimate the yield strain to be of order $\varepsilon_y \approx 0.01$, beyond which the plant tissue will be irreversibly deformed.

In reality, if the change in force is applied sufficiently slowly, then plants can avoid breakage by either growing (in cell number or cell size) or toughening the cell wall [4]. In this model, we assume that the plant material properties remain constant. Growth reduces the strain to a level $\varepsilon_g < \varepsilon_y$, thus preventing the material from breaking, and permitting growth to still larger sizes. To mimic the natural response of biological materials to external forces, we replace ε_y with ε_g in Eq. (2). Because the growth response is associated with positive strain, we assume in our model that compression does not generate yielding. The pumpkin material elasticity $E \approx 1$ MPa has been measured by previous tests [31]; the critical tensile strain leading to growth, ε_g, will be estimated using our modeling.

Using dimensional analysis, we write the height H/L of the pumpkin as a function of three dimensionless groups: these include the growth strain ε_g, the dimensionless thickness t/L, and ratio of the pumpkin's weight to elastic forces, $\rho g L/E$. The problem of determining the pumpkin's height reduces to using experiments to obtain the relation

$$\frac{H}{L} = f\left(\varepsilon_g, \frac{t}{L}, \frac{\rho g L}{E}\right). \tag{3}$$

In our study, the pumpkin material, with Young's modulus E and Poisson's ratio ν, is represented by a network of springs with Hooke's constant k connecting nodes (point masses M). We simulate growth by increasing the mass, and thus the gravitational force, of all nodes in the pumpkin. Increases in weight will necessarily generate elastic deformation of the pumpkin corresponds to compression and stretching of the springs. Further deformation is induced by plastic yielding of the network. Plastic yielding at strains of ε_g corresponds to increases in the spring rest length r^{eq}, which mimics anomalous growth (the addition of new cells and cellular growth at points of yielding [9]).

The elastic energy associated with a node at position $\boldsymbol{r}_i$ is $E_s(\boldsymbol{r}_i) = \frac{1}{2}\sum_j k_{ij}(r_{ij} - r_{ij}^{eq})^2$ (see Fig. 4). Here, $r_{ij} = |\boldsymbol{r}_i - \boldsymbol{r}_j|$ is the length of the spring between two nodes with positions $\boldsymbol{r}_i$ and $\boldsymbol{r}_j$, $\boldsymbol{r}_{ij}^{eq}$ is its equilibrium length, and k_{ij} is the stretching spring constant. This results in a spring force $\boldsymbol{F}_s = \partial E_s/\partial \boldsymbol{r}_i$. The dynamics of the solid material is captured by integrating Newtons equation of motion $\boldsymbol{F}(\boldsymbol{r}_i) = M_i \partial^2 \boldsymbol{r}_i/\partial t^2$, using the velocity Verlet algorithm [36] which is commonly used in molecular dynamic simulations [37]. Here, $\boldsymbol{F}$ is the total force acting on the node, which consists of the spring force, the force due to shell-wall interactions, and a dissipative force proportional to the node translational velocity. The latter force is included to suppress elastic oscillations excited due to shell deformations which are quasi-static in practice. We have verified that this dissipative force is weak enough not to affect the shape evolution.

For elasto-plastic materials when the material stress σ reaches the yield magnitude σ_y, the material starts deforming plastically at constant stress. In our computational model, we mimic this plastic behavior by dynamically changing the equilibrium spring length r^{eq} of individual springs. Specifically, when material strain $\varepsilon = (r - r^{eq})/r^{eq}$ exceeds the critical level ε_g, we assign a new value to the equilibrium length $r_{new}^{eq} = r^{eq}(\varepsilon + 1)/(\varepsilon_g + 1)$. We introduce plasticity only for positive strains, i.e. when the material is stretched, while the compression is completely elastic.

The pumpkins three-dimensional shell (Fig. 4) is constructed from four concentric layers of LSM nodes [38]. Using the Delaunay triangulation technique [39], we distribute nodes in a regular manner on each concentric layer. The layers are separated by a distance that is equal to the average size of a triangular bond Δx and are connected by springs between the nearest and next-nearest neighbour nodes, with spring constants k and $2/3k$, respectively. For this arrangement of nodes and springs, the Young's modulus of the solid is approximately given by $E = 5k/2\Delta x$, the Poisson's ratio is $\nu = 0.25$ (which is consistent with that found for typical plant materials, e.g. [30]) and the solid density is $\rho = 2M/\sqrt{3}\Delta x^3$. In our simulations, the outside diameter of the undeformed pumpkin is $L = 40$, the density is $\rho = 1$,

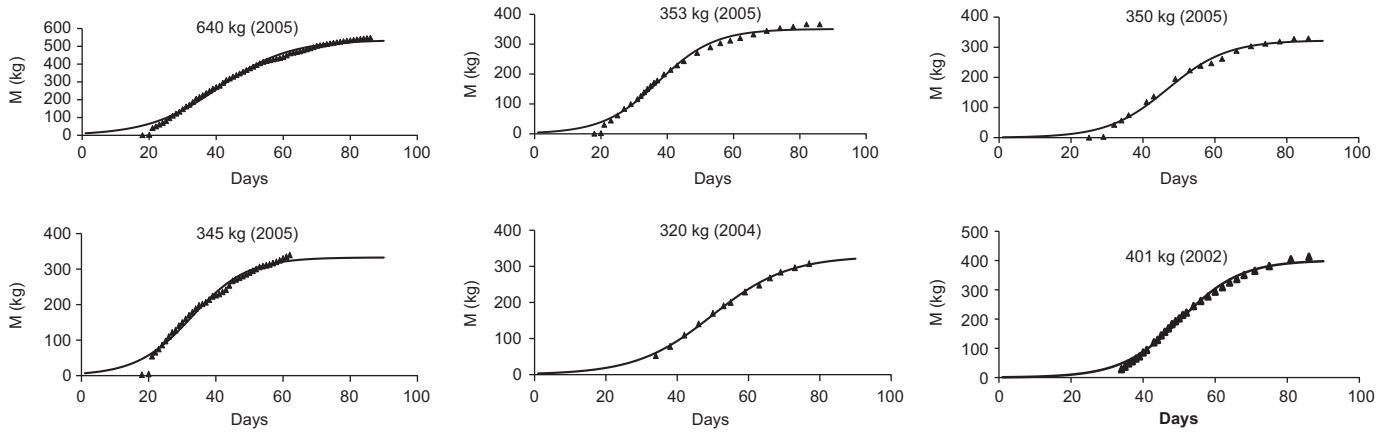

Fig. 5. The relation between time and weight for giant pumpkins grown by Andy Wolf in years 2002–2005.

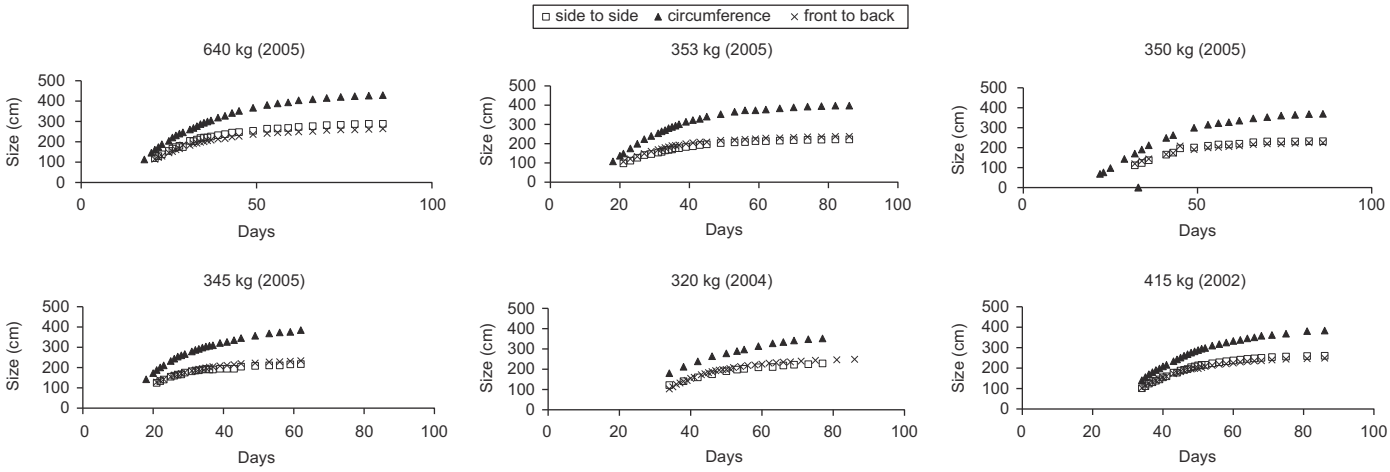

Fig. 6. Relation between time and three measures of circumference (horizontal circumference, side-to-side and front-to-back measurements). Pumpkins grown by Andy Wolf in years 2002–2005.

and the modulus is $E = 5/18$, where values are given in lattice-spring units. The number of LSM nodes in each layer[1] is $N = 2562$, the average spacing between nodes is $\Delta x \approx 0.033L$, and the thickness of the shell is $t = 0.14L$.

We have validated our LSM simulation by breathing-mode oscillations of the spherical shell and found excellent agreement with theoretical results [40]. We have also found good agreement with the experimental data we collected from the compression Instron experiments with different pumpkins. Furthermore, we have verified that the change in grid resolution of our computational model practically does not affect the simulation results, indicating that the computational grid is sufficient to resolve plastic deformation of pumpkins.

3. Results

3.1. Weight and geometry change

Fig. 5 show the relation between weight and time for six giant pumpkins grown between 2002 and 2005 by Andy Wolf. Graphs are labeled according to the final weight of the pumpkin and the year the pumpkin was grown; time $t=0$ corresponds to anthesis. The mass M is described by a sigmoid function,

$$M = c/(1+de^{-ft}) \tag{4}$$

where t is time, and c,d,f are constants. Using least-square analysis, we find that $c = 380 \pm 80$ kg, $d = 169 \pm 150$, and $f = 0.11 \pm 0.01$ s^{-1}. The constants c and d provide the initial mass measured ($M(t=0) = c/(1+d) \approx 2.2$ kg, the position of the inflection point ($t_{inflection} = (\ln d)/f \approx 51$ days) and the final mass of the pumpkin ($M(t=\inf) = c \approx 380$ kg). It is noteworthy that f is constant across a broad range of final weights (320–640 kg).

Fig. 6 shows the relation between the three circumferences of the pumpkin (one horizontal and two vertical). Clearly, the vertical circumferences are similar indicating that growth is roughly axisymmetric (where the axis is tangent to gravity and intersecting the center of the pumpkin). The gradual increase of the horizontal circumference over the vertical circumferences shows that the pumpkins are gradually becoming squashed as they grow.

Fig. 7a shows the relation between dimensionless thickness t/L and diameter L. Crosses represent the minimum thickness t_{min}/L, while circles represent the maximum thickness t_{max}/L. Using least-squares fit, we find that the maximum thickness increases linearly with L, whereas the minimum thickness decreases with L. In small pumpkins, thickness appears relatively uniform, as shown by the similarity between minimum and maximum thickness on the left-hand side of Fig. 7a. Large pumpkins exhibit a

[1] Note that it would be computationally impossible for each cell in the fruit to be represented by a separate node. For example, a mature apple has 40 million cells, following over 20 doublings by cell division [28].

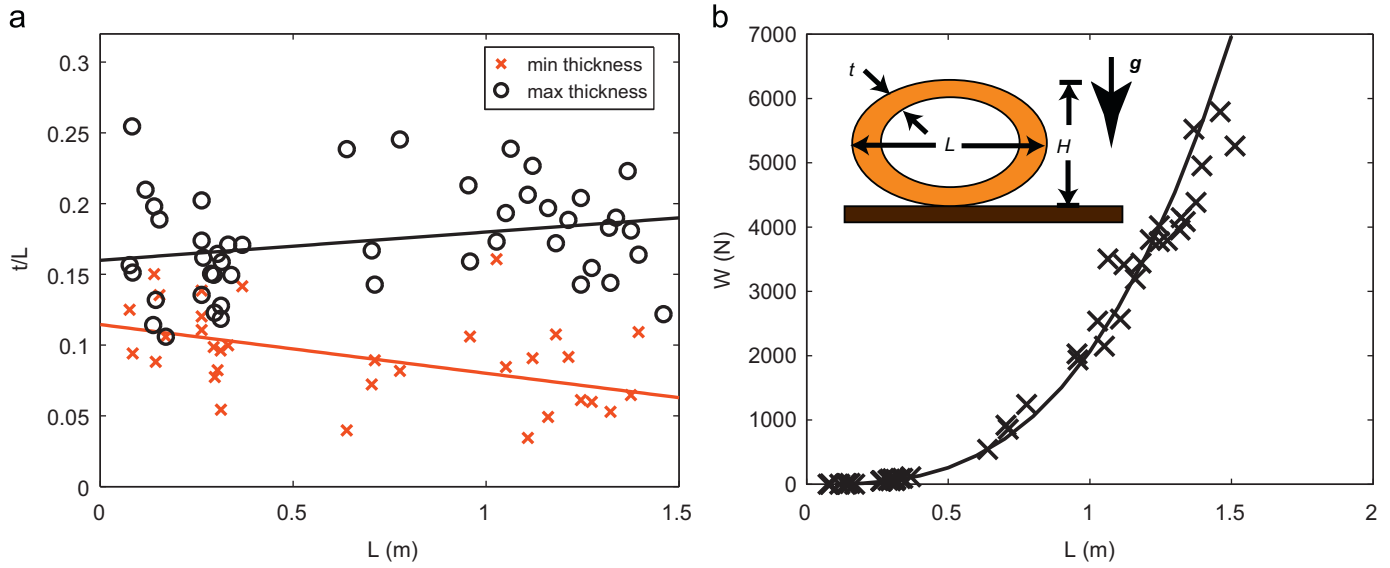

Fig. 7. (a) The relation between dimensionless thickness t/L and pumpkin diameter L. Red crosses and black circles represent the minimum and maximum thickness on the pumpkin, respectively. The best fit lines, calculated using least-squares, correspond to $t_{min}/L = -0.03\ \mathrm{L} + 0.11$ ($N = 35$, $R^2 = 0.26$) and $t_{max}/L = 0.02\ \mathrm{L} + 0.16$ (L in meters, $N = 49$, $R^2 = 0.07$) where units of L are in meters. (b) The relation between pumpkin diameter L and weight W. The solid line shows the fit given by Eq. (5) in which $W \sim L^3$. Inset of (b) shows a schematic of the model pumpkin. The pumpkin has a diameter L, thickness t and height H; its material properties are described by a density ρ and elasticity E; and it grows under influence of gravity (acceleration g). (For interpretation of the references to color in this figure legend, the reader is referred to the web version of this article.)

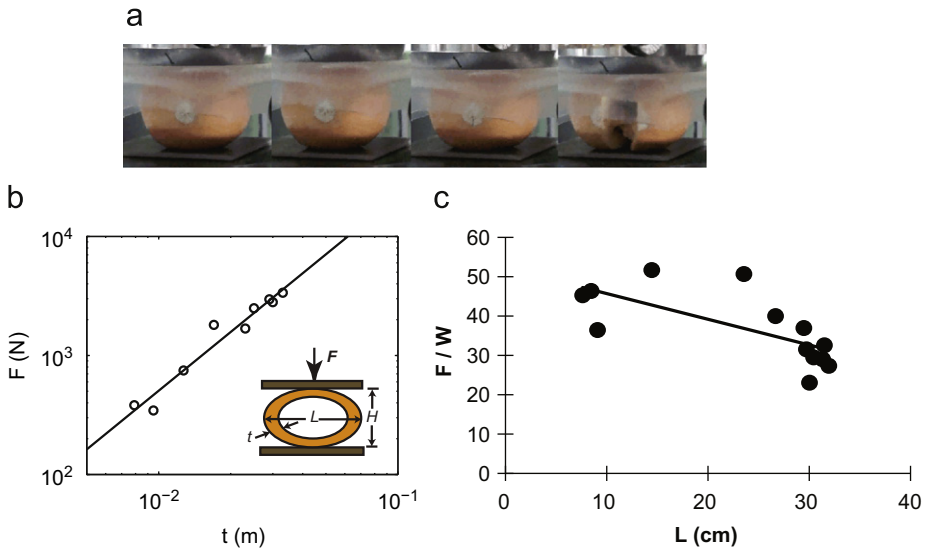

Fig. 8. (a) Time-lapse photographs of a pumpkin crushed in the Instron materials tester. (b) Force F required to break a pumpkin of thickness t, squeezed between two plates. The least-squares best fit shown is given by $F \sim t^{1.5}$. (c) The relation between pumpkin diameter and ratio of breaking force to weight (F/W).

greater variability in thickness, indicating that growth varies spatially along the pumpkin. For the purpose of our modeling, we approximate the growing pumpkin as having uniform thickness $t = 0.14L$, approximately the average thickness observed.

Fig. 7b plots the weight W of pumpkins as a function of their diameter. The data is fit by the weight of a spherical shell with uniform thickness, $W = \pi/6\rho g L^3(1-(1-2t/L)^3)$ where assuming a constant ratio t/L leads approximately to the trends observed, $W \sim L^3$, or specifically,

$$W = aL^b \tag{5}$$

where W is in Newtons and L in meters, $a = 2070$, $b = 3.0$ ($N = 49$, $R^2 = 0.97$). We note that the discrepancy between the model and data for larger pumpkins can be attributed to deformation of the shell.

3.2. Breaking force

For sufficiently thin elastic shells ($t \ll L$), the breaking force F of a spherical shell is well-known. The force scales according to $F \sim \sigma_f t^2$, where σ_f is the breaking stress of the shell; this result that has been shown both theoretically [41] and by breaking hundreds of eggshells [42]. According to our breaking experiments (Fig. 8), we find pumpkins follow a different trend presumably because they are thick-walled: using a least-squares fit, the breaking force $F = at^b$ where F is in Newtons, t in meters,

$a = 2.9 \times 10^5$ N/m$^{3/2}$ and $b = 1.5$ ($N = 7$, $R^2 = 0.96$). Assuming pumpkins have a uniform thickness of $t = 0.14L$, we can estimate their maximum size. This occurs at a diameter $L_{max} \approx 1.5 \times 10^3 (\rho g)^{-1.5} \approx 3.3$ m and a corresponding pumpkin mass of 9000 kg. However, non-uniformities of the pumpkin shell, as we observed, may lead to breaking at smaller sizes. For example, pumpkin density ρ can increase suddenly during rainstorms, after which pumpkin explosions have been documented [43]. Even if mechanical failure does not occur due to material breakage at these sizes, plastic deformations associated with pumpkin growth will affect pumpkin development.

Fig. 8a shows a market pumpkin slowly crushed between two plates. This process is analogous to a pumpkin increasing in weight, and we use the experiment to estimate the maximum weight of a pumpkin before it fractures from self-weight. This experiment provides an important control test: this is the weight pumpkins would grow if they were unable to plastically deform and so reduce local stresses. Fig. 8c shows the relation between pumpkin diameter and the maximum non-dimensionalized compressive force that the pumpkin can support (F/W). The linear fit is: $F/W = -0.65L + 52$, with L in cm ($R^2 = 0.47$). Without the assistance of growth-mediated plasticity, breakage ($F/W = 1$) should occur at a size $L_{max} = 79$ cm. To make a more reliable estimate using this method, more data is required. We note that this estimate is about half of the current world record value, $L = 1.4$ m. The discrepancy between these two values indicates the importance of considering plastic deformation.

3.3. Observed plastic deformation

As shown by the time-lapse photographs in Fig. 9a and by the circular symbols in Fig. 10, as the pumpkin increases in size from $L = 3$ to 140 cm (or its dimensionless weight $\rho gL/E$ increases from 0.0001 to 0.01), the aspect ratio of the pumpkins can decrease as much as 50%. This was manifested visibly in Fig. 3, in which small pumpkins ($L < 50$ cm) were generally spherical, while large pumpkins ($L > 1$ m) appeared squashed. This flattening occurs primarily due to deformation at the base of the pumpkin.

According to thin-shell theory [44,41,45], the region of greatest tensile stress occurs on the bottom of the pumpkin, which supports most of the pumpkin's weight, $W \sim \rho g L^2 t$. This force is applied at a distance $L/2$ from the pumpkin's center of mass, and generating a torque $\tau \sim (L/2)\rho g L^2 t$. The peak bending stress at the edge of the shell is given by $\sigma_{max} = 2\tau/(t^2 L)$. The associated strain is given by $\varepsilon_{max} = \sigma_{max}/E \sim (L/t)(\rho g/E)L \sim 1-10\%$ which suggests that the largest pumpkins will suffer plastic deformation at their bases. To determine more precisely the effect of plastic deformation, we turn to our computational model.

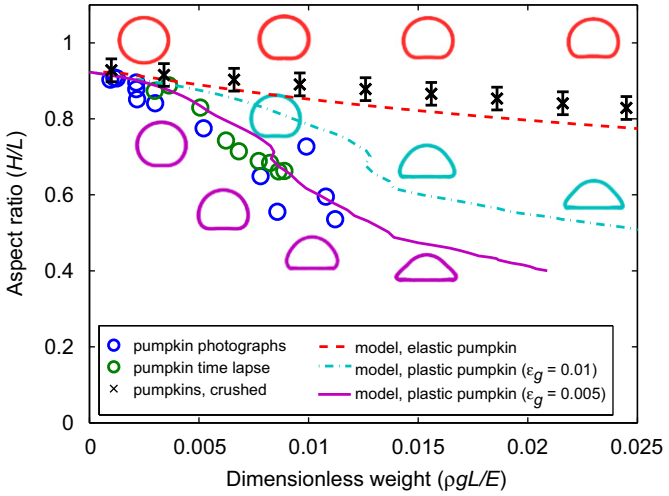

Fig. 10. The relation between pumpkin aspect ratio H/L and dimensionless pumpkin weight $\rho gL/E$. Circular symbols represent deformations of growing pumpkins (with blue circles provided by pumpkin photographs by volunteer farmers and green circles provided by time-lapse images donated by [34]. Crosses represent deformations of pumpkins squeezed in an Instron machine with a dimensionless force $\rho gL/E$, as in Fig. 8. Error bars represent standard errors of measurement. The curves represent pumpkin deformation models incorporating elasticity $E \approx 1$ MPa (dashed curve) and plastic yield strain (dash-dot curve), and growth yield strain (solid curve). Note that the elasto-plastic pumpkin deforms five times as much as the elastic pumpkin, given the same gravitational load. Insets show the approximate deformation of pumpkins using these three models. (For interpretation of the references to color in this figure legend, the reader is referred to the web version of this article.)

Fig. 9. Time-lapse photographs of a growing giant pumpkin, courtesy of Ryan Foss [34].

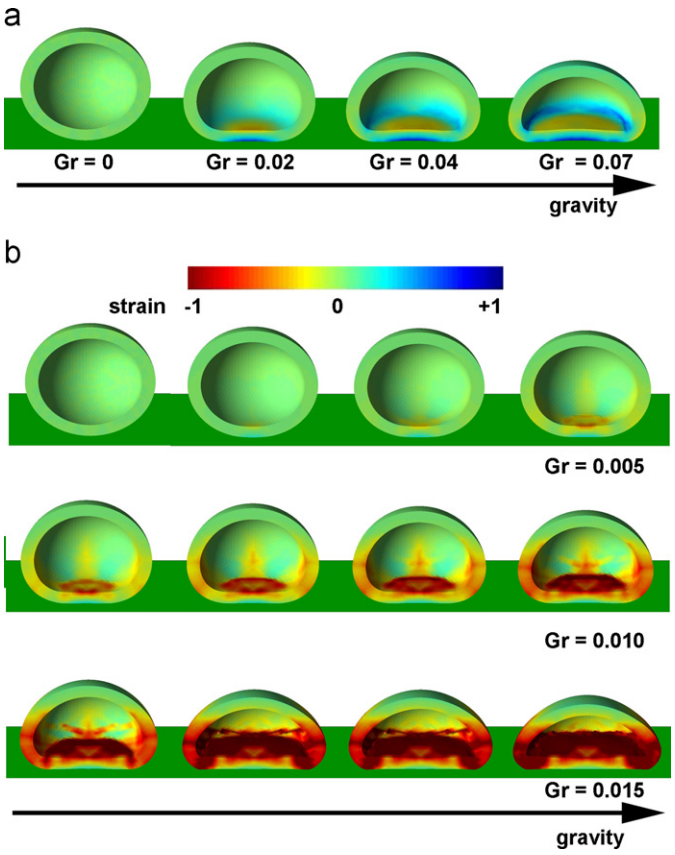

Fig. 11. Simulations of pumpkin growth for (a) an elastic pumpkin (with no plastic deformation) and (b) a elasto-plastic pumpkin (with plastic yield of 0.005). Color indicates the sign of the strain: green (zero strain), blue (tensile strain), red (compressive strain). Note that the elasto-plastic pumpkin deforms five times as much as the elastic pumpkin, given the same gravitational load. (For interpretation of the references to color in this figure legend, the reader is referred to the web version of this article.)

3.4. Computed pumpkin shapes

Using our computational model, we calculate pumpkin shapes (Fig. 11) and heights (lines in Fig. 10). In the sequence of pumpkin shapes, blue color denotes compression; red color denotes tension. The dashed curves shows pumpkin height due to elasticity alone. The dash-dot and solid curves shows the height due to elasto-plastic behavior (defined in Eq. (2)) using the values of the growth strain $\varepsilon_g = 0.01$ and 0.005, respectively. In our numerical method, forces were applied to virtual pumpkins that were initially nearly spherical ($H/L \approx 0.9$, which is close to the shape of the pumpkins we measured). The elastic deformation model (red line) is roughly linear in the range of weights measured. However, we find that the evolution of plastic deformation is non-linear. Specifically, the shell exhibits rapid changes in height at $W = 0.0113$ and 0.008 for the growth strains $\varepsilon_g = 0.01$ and $\varepsilon_g = 0.005$, respectively. These shape changes are associated with plasticity-induced buckling of the shell. Because of the coarseness of our experimental data, it is not clear whether such buckling occurs in nature.

Our elastic model provides a good estimation of forces applied very quickly to a pumpkin, as shown by correspondence between the cross symbols, representing instron crushing experiments, and the dashed curve in Fig. 10. We conclude that forces applied quickly to pumpkins causes them to respond elastically before rupture. The elastic forces, however, are insufficient to generate the substantial deformations observed in growing pumpkins. In growing pumpkins (in the size range $\rho gL/E < 0.01$), aspect ratio decreases by 40%, with only 10% due to elastic forces.

The incorporation of a plastic yield stress into our elastic model, as in Eq. (2), allows us to predict pumpkin heights consistent with those observed, as shown by the correspondence between the circular symbols and the solid curve in Fig. 10. We find that pumpkin shapes are best approximated using a yield strain $\varepsilon_g = 0.005$, which is about half of the plastic limit ε_y of plant cells [30]. Calculations of stress in the pumpkin material shown in Fig. 11 reveal meridians of high tensile stress (seen by the vertical red lines at $\rho gL/E = 0.01$), which are consistent with the formation of vertical cracks in the ribs of the pumpkin, as observed by farmers. We note that the elasto-plastic model shows sensitivity to changes in the yield strain ε_g. Specifically, when we reduce ε_g from 0.005 to 0.001, we observe taller pumpkins and a much poorer correspondence to the heights observed, as shown by the dash-dot line in Fig. 10.

3.5. Predicting maximum pumpkin size

What is the largest pumpkin that can be grown? This is a difficult question for several reasons. First, as shown in Fig. 2, giant pumpkins are the fastest growing of all fruits. This makes it difficult to obtain growth limits using comparisons to other fruits. Second, the growth process involves many biological factors that we do not consider in our study, such as the role of genetics, growing techniques and resources supplied. It is likely that these variables will play a role in constraining growth. In this section, we highlight a potential mechanical problem that may arise at large sizes.

Predicting fracture due to self-weight can be approached from the perspective of force or time. In our present investigation, we have shown that pumpkins can readily deform in response to sufficiently large local stresses: the result of this response is the observed flattened shape of pumpkins. It is noteworthy that only a 0.005 yield strain can lead to reduction in pumpkin height of 40%. We now briefly discuss the role of growth rates in limiting the size of pumpkins.

In our current modeling efforts, we make no reference to how quickly pumpkins can plastically deform during growth. In discussions with growers, we find that pumpkins tend to form cracks during the fastest part of the growing season (around day 50 in Fig. 5) and during the fastest changes in water content (e.g. rainstorms). Farmers have stated that pumpkins can grow in weight by up to 15 kg per day. After harvesting, pumpkins lose 2 kg of water per day alone due to evaporation. The majority of these weight gains and losses are due to water uptake.

The total growth rate of the pumpkin is due to cellular division and expansion. It can be measured as the rate of increase in relative distance between two painted spots on the pumpkin. We approximate the total growth rate using two components: the first due to uniform increase in size and the second due to plastic deformation of the pumpkin:

$$\dot{\varepsilon}_{total} = \dot{\varepsilon}_{uniform} + \dot{\varepsilon}_{def} \tag{6}$$

We can estimate uniform growth rate, $\dot{\varepsilon}_{uniform}$, using the grower's measurements for (c,d,f), given in Eq. (4) and Fig. 5. For modeling the growth of larger pumpkins, we adjusted the value of c according to the corresponding final pumpkin mass; we left the remaining constants d and f as measured. The deformation growth rate, $\dot{\varepsilon}_{def}$ may be estimated using our simulations in combination with (4). We examined all nodes in our computational pumpkin to find the point of largest plastic deformation for a given pumpkin weight. We find that the maximum plastic deformation in the pumpkin is given by

$$\varepsilon_{def} = j e^{k\overline{W}} \tag{7}$$

where $j = 0.0144$, $k = 308$ and $\overline{W}$ is the dimensionless weight. The fit of this equation to our numerical solution is shown in Fig. 12a ($R^2 = 0.88$). The question that arises then is: can the pumpkin's cells

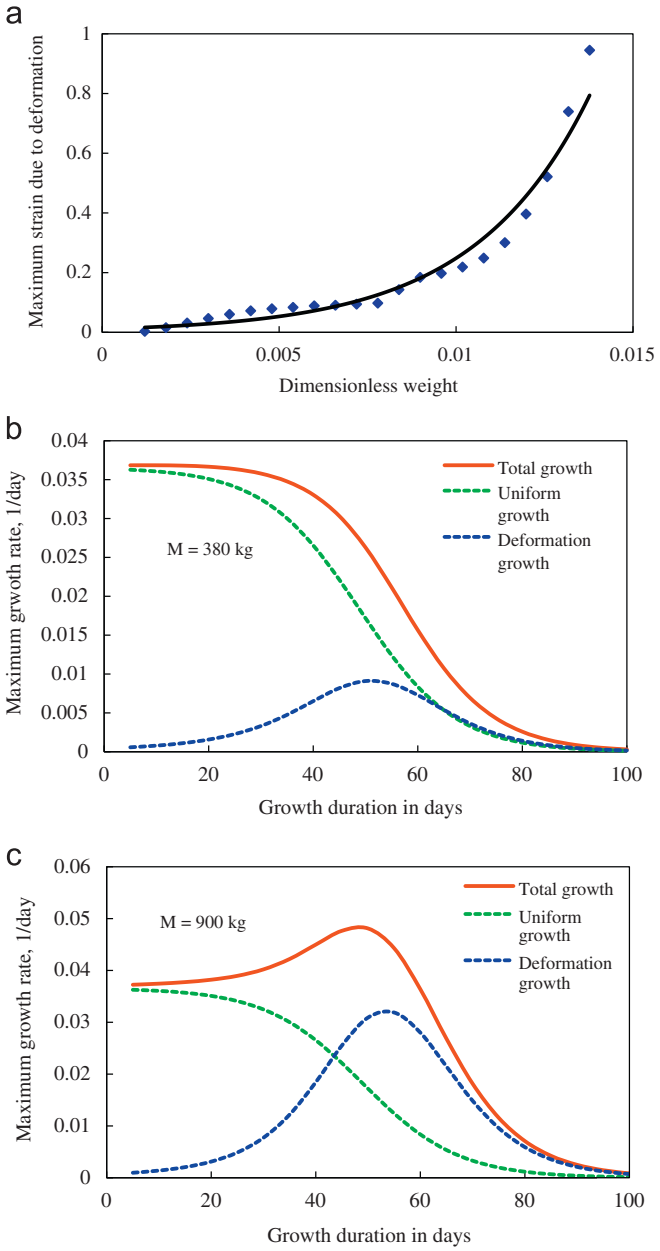

Fig. 12. (a) The relation between maximum deformation strain and dimensionless weight, as calculated using our model. Note that as weight increases, so does the strain. (b–c) The relation between time and growth rate. Calculations are shown for two pumpkins, one of 380 kg (b) and the other of 900 kg (c).

grow (divide and expand) sufficiently quickly to accommodate the pumpkin deformation?

Fig. 12b–c shows the maximum growth per day across the growth season for two pumpkins of final weights 380 and 900 kg, respectively. For moderately sized giant pumpkins ($M = 380$ kg, Fig. 12b), the uniform growth rate (with a maximum value of 0.035 day^{-1}) is much larger than the deformation growth rate (with a maximum value of 0.01 day^{-1}). At day 50, the pumpkin has a uniform growth of 0.02 day^{-1} and thus, an increase in weight of $1.02^3 \approx 6\% \approx 9$ kg day^{-1}, as is consistent with farmer's observations. During this peak in mass added per day, the deformation growth is also at its largest (at 0.01 day^{-1}). Certain parts of the pumpkin are thus forced to grow at a combined rate of nearly 0.035 day^{-1} during the peak of the growth season. For pumpkins of moderate size, the deformation does not significantly affect the total growth rate.

For heavier pumpkins such as the 900-kg pumpkin (the world record for 2010) shown in Fig. 12c, the total growth rate can reach values of 0.05 day^{-1}. The maximum growth rate is obtained at day 50, where the deformation growth rate has in fact exceeded the uniform growth rate. This high value may be limiting to plant tissue. Roots are known to exhibit strains up to 0.5 h^{-1} in maize root [46], but fruit cells are unlikely to grow so quickly. Thus, at large weights during the peak of the growth season, pumpkins may be unable to grow to reduce local stresses and may be prone to fracture instead.

4. Conclusions

In this combined experimental and theoretical study, we investigated the shape evolution of giant fruits. We collected pumpkin growth data from fifty volunteer farmers and compared this data to the predictions of our computational model. Using Instron materials assays, we measured the fracture force of normal-sized pumpkins, which enabled us to make estimates of their maximum size before fracture under self-weight. In our computational model, we predicted the deformed shapes of giant pumpkins using a single free parameter, the growth strain ε_g, which we found to be 0.005. It is noteworthy that the growth strain is less than the yield strain of pumpkin tissue ($\varepsilon_g < \varepsilon_y$), as expected, indicating that pumpkins will tend to avoid crack formation via increased rates of localized cell division.

Giant pumpkin shapes are more diverse than we are able to account for with our current model. First, our model only predicts convex pumpkin shapes. However, large pumpkins sometimes exhibit a curvature reversal at their base. This phenomenon is likely related to the high tensile stresses we computed at the base of the pumpkin (red regions in Fig. 11). Farmers have circumvented such pumpkin deformities by growing them on slippery vinyl to decrease the coefficient of friction of the pumpkin. Second, our model assumes that pumpkin thickness is uniform, as in market pumpkins. However, large pumpkins appear to exhibit a distribution of thicknesses throughout the shell, as shown in Fig. 7. This variability in growth might be caused by the presence of the flowering and stem ends of the fruit which may create an asymmetric transmission and distribution of water and nutrients. Third, our model assumes homogeneous material properties, but the pumpkin skin is clearly more stiff than the interior flesh. A gradient model or multilayer model may work better, which can take into account inhomogeneities in elastic moduli and yield stress. We hope that models of further complexity can predict these and other interesting growth phenomena that we were unable to explain here.

The limits of our study highlight the many open questions remaining in the study of giant plant growth. The growth of plants to extreme sizes, while requiring specialized farming methods, can help to answer biological questions that are impossible to address using normal-sized plants. We hope that the Atlantic giant pumpkin will continue to serve future workers, as it did the authors, as both a model organism and a source of wonder.

Acknowledgements

The authors thank K. Kim for preparing Figures 1–2, R. Amaro and G. Russell for assistance with Instron experiments and M. Shelley for useful discussions. Pumpkin measurements were donated by the members of Bigpumpkins.com, NEPGA (the New England Pumpkin Grower's Association), and Great Pumpkin Commonwealth (GPC), with special thanks to A. Wolf, L. Stellplfug,

S. Jepsen, A. Nesbitt, J. Peek, M. Lombardi, B. Bortner, F. Buglio, T. Brownell, E. Robinette, B. Buchsieb, J. Vandrey, S. Tanner, W. Horton, C. Revier, J. Gerchy, C. Brigitte, T. White, A. Macarchuk, A. Nesbitt, W. Brandon, R. Stidwill, B. King, J. Ciesielski, S. Armstrong, M. Strange and V. Zunino.

References

[1] J.A. Thomson, On growth and Form, Nature 100 (1917) 21–22.
[2] K.E. Koch, Carbohydrate-modulated gene expression in plants, Annual Review of Plant Biology 47 (1) (1996) 509–540.
[3] T.I. Baskin, Anisotropic expansion of the plant cell wall, 2005.
[4] L. Taiz, Plant cell expansion: regulation of cell wall mechanical properties, Annual Review of Plant Physiology 35 (1) (1984) 585–657.
[5] A. Goriely, M. Robertson-Tessi, M. Tabor, R. Vandiver, Elastic growth models, Applied Optimization 12 (2008) 1–44.
[6] L.A. Taber, Biomechanics of growth, remodeling, and morphogenesis, Applied Mechanics Reviews 48 (1995) 487.
[7] R. Vandiver, A. Goriely, Tissue tension and axial growth of cylindrical structures in plants and elastic tissues, EPL (Europhysics Letters) 84 (2008) 58004.
[8] J. Dumais, S.L. Shaw, C.R. Steele, S.R. Long, P.M. Ray, An anisotropic-viscoplastic model of plant cell morphogenesis by tip growth, International Journal of Developmental Biology 50 (2) (2006) 209–222.
[9] E. Coen, A.G. Rolland-Lagan, M. Matthews, J.A. Bangham, P. Prusinkiewicz, The genetics of geometry, Proceedings of the National Academy of Sciences 101 (14) (2004) 4728–4735.
[10] G.A. Buxton, C.M. Care, D.J. Cleaver, A lattice spring model of heterogeneous materials with plasticity, Modelling and Simulation in Materials Science and Engineering 9 (6) (2001) 485–497.
[11] A.J.C. Ladd, J.H. Kinney, T.M. Breunig, Deformation and failure in cellular materials, Physical Review E 55 (3) (1997) 3271–3275.
[12] M. Born, The crystal lattice theory of diamonds, Annalen Der Physik 44 (12) (1914) 605–642.
[13] M. Ostoja-Starzewski, P.Y. Sheng, K. Alzebdeh, Spring network models in elasticity and fracture of composites and polycrystals, Computational Materials Science 7 (1–2) (1996) 82–93.
[14] A. Alexeev, A.C. Balazs, Designing smart systems to selectively entrap and burst microcapsules, Soft Matter 3 (12) (2007) 1500–1505.
[15] A. Levandovsky, A.C. Balazs, Mechanisms for fragment formation in brittle solids, Physical Review E 75 (5) (2007) 056105.
[16] G.W. Koch, S.C. Sillett, G.M. Jennings, S.D. Davis, The limits to tree height, Nature 428 (6985) (2004) 851–854.
[17] D.L. Hu, B. Chan, J.W.M. Bush, The hydrodynamics of water strider locomotion, Nature 424 (2003) 663–666.
[18] R.M. Alexander, Principles of Animal Locomotion, Princeton University Press, 2003.
[19] R. Dudley, The evolutionary physiology of animal flight: paleobiological and present perspectives, Annual Review of Physiology 62 (2000) 135–155.
[20] N. McWhirter, Guinness Book of World Records, Bantam Books, 2004.
[21] K. Hartman, National register of big trees, American Forests 88 (4) (1982) 17–31.
[22] C.J. Earle, The Gymnosperm Database 2006.
[23] D. Langevin, How-to-Grow World Class Giant Pumpkins, Annedawn Publishing, 1993.
[24] J. Yin, Z. Cao, C. Li, I. Sheinman, X. Chen, Stress-driven buckling patterns in spheroidal core/shell structures, Proceedings of the National Academy of Sciences 105 (49) (2008) 19132–19135.
[25] E.W. Sinnott, A developmental analysis of inherited shape differences in Cucurbit fruits, American Naturalist (1936) 245–254.
[26] E.W. Sinnott, The genetic basis of organic form, New York Academy Sciences Annals 71 (1958) 1223–1233.
[27] E.W. Sinnott, A developmental analysis of the relation between cell size and fruit size in cucurbits, American Journal of Botany (1939) 179–189.
[28] B.G. Coombe, The development of fleshy fruits, Annual Review of Plant Physiology 27 (1) (1976) 207–228.
[29] R. Bernal, E.R. Rojas, J. Dumais, The mechanics of tip growth morphogenesis: what we have learned from rubber balloons, Journal of Mechanics of Materials and Structures 2 (2007) 1157–1168.
[30] K.J. Niklas, Plant Biomechanics: An Engineering Approach to Plant Form and Function, University of Chicago Press, 1992.
[31] L. Mayor, R.L. Cunha, A.M. Sereno, Relation between mechanical properties and structural changes during osmotic dehydration of pumpkin, Food Research International 40 (4) (2007) 448–460.
[32] J.A. Lockhart, An analysis of irreversible plant cell elongation, Journal of Theoretical Biology 8 (2) (1965) 264–275.
[33] A.G. Calbo, J.D.C. Pessoa, A plant growth re-analysis. An extension of Lockhart's equation to multicellular plants, Revista Brasileira de Fisiologia Vegetal 6 (1994) 83–90.
[34] R. Foss, B. Nagel, Bill's Big Pumpkins, a Quantum Petshop Documentary, 2007.
[35] A. Nawirska, A. Figiel, A.Z. Kucharska, A. Sokol-Letowska, A. Biesiada, Drying kinetics and quality parameters of pumpkin slices dehydrated using different methods, Journal of Food Engineering 94 (1) (2009) 14–20.
[36] L. Verlet, Computer experiments on classical fluids. Part I. Thermodynamical properties of Lennard–Jones molecules, Physical Review 159 (1) (1967) 98–103.
[37] D. Frenkel, B. Smit, Understanding Molecular Simulation: From Algorithms to Applications, second ed., Academic, San Diego, California, London, 2002.
[38] A. Alexeev, R. Verberg, A.C. Balazs, Patterned surfaces segregate compliant microcapsules, Langmuir 23 (3) (2007) 983–987.
[39] B.N. Delaunay, Sur la sphere vide, Bulletin of the Academy of Science of the USSR: Class des Sciences Mathmatique et Naturelles 7 (6) (1934) 793–800.
[40] A. Alexeev, R. Verberg, A.C. Balazs, Modeling the motion of microcapsules on compliant polymeric surfaces, Macromolecules 38 (24) (2005) 10244–10260.
[41] C.R. Steele, Asymptotic analysis and computation for shells, in: A.K. Noor, T. Belytschko, J.C. Simo (Eds.), Analytical and Computation Models of Shells, American Society of Mechanical Engineers, New York, 1989, pp. 3–31.
[42] A. Ar, H. Rahn, C.V. Pagnelli, The avian egg: mass and strength, Condor 81 (1979) 331–337.
[43] J. Gold, Exploding pumpkins, National Public Radio, 2008.
[44] W. Flügge, Stresses in Shells, Springer-Verlag, New York, 1973.
[45] J. Heyman, The Stone Skeleton: Structural Engineering of Masonry Architecture, Cambridge University Press, Cambridge, UK, 1995.
[46] W.G. Spollen, R.E. Sharp, Spatial distribution of turgor and root growth at low water potentials, Plant Physiology 96 (2) (1991) 438.